Inorganic Chemistry

Article

pubs.acs.org/IC

Photochromogenic Nanosheet Crystallites of Tungstate with a 2D Bronze Structure

Katsutoshi Fukuda,*[,†] Kosho Akatsuka,[†] Yasuo Ebina,[†] Minoru Osada,[†] Wataru Sugimoto,[‡] Mutsumi Kimura,[‡] and Takayoshi Sasaki*[,†]

[†]International Center for Materials Nanoarchitectonics (MANA), National Institute for Materials Science, 1-1 Namiki, Tsukuba, Ibaraki 305-0044, Japan

[‡]Faculty of Textile Science and Technology, Shinshu University, 3-15-1 Tokida, Ueda, Nagano 386-8567, Japan

ABSTRACT: Layered rubidium tungstate, $Rb_4W_{11}O_{35}$, with a two-dimensional (2D) bronze-type tunnel structure was successfully delaminated into colloidal nanosheets via a soft-chemical process involving acid exchange and subsequent intercalation of tetrabutylammonium ions. Characterizations by transmission electron microscopy and atomic force microscopy confirmed the formation of unilamellar 2D nanosheet crystallites with a unique thickness of ~3 nm and an average lateral size of 400 nm. The obtained nanosheets exhibited reversible color change upon UV-light excitation via an optical band gap of 3.5 eV. The ultimate 2D aspect ratio favorable for an adsorption of charge-compensating cations to trapped electrons working as a color center is presumably responsible for highly efficient photochromic behavior. Its coloration mainly consists of a broad band at a wavelength of 1800 nm and longer, which is much different from that of the common tungstate nanomaterials. Thus, the chromogenic nanosheet obtained in this study features the intense UV absorption and optically switchable visible-to-IR absorption, which may be useful for window applications such as cutoff filters and heat-absorbing films.

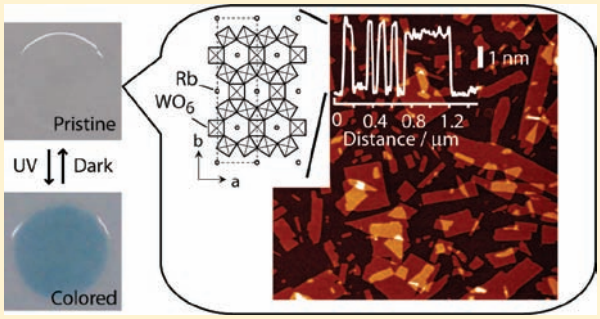

INTRODUCTION

A series of tungsten oxides has been investigated as a class of versatile materials with a range of functionalities, e.g., semiconducting,[1] ferroelectric,[2] superconducting,[3] and photo- and electrochromic[4,5] properties. Above all, the chromic behavior observed in amorphous and bronze-type tungstates is of particular interest for optics- and energy-related applications.[4c,6,7] The coloration of these tungstates, which is believed to be induced by intervalence charge-transfer transition between localized W^{4+}, W^{5+}, and W^{6+} states, involves the adsorption of charge-compensating cations to trapped electrons as a color center, i.e., *double injection*. Thus, the performance strongly depends on the presence of surface sites, and many attempts have been made to downsize them to enhance the surface area over the past decades.

One of the unique and efficient approaches to downsize material dimensions is the exfoliation of layered compounds into elementary host layers.[8−11] The resultant unilamellar crystallites, called nanosheets, are a unique class of low-dimensional nanomaterials with a nanometer-scale thickness and a lateral size typically on the scale of micrometers. Such a two-dimensional (2D) anisotropy ultimately provides extensive sites accessible for adsorbents, making the nanosheet particularly favorable for photochromism governed by *double injection* at the surface. The exfoliation technique can, therefore, be considered as a promising method in developing highly efficient inorganic photochromogens. However, except for our recent report on the tungstate nanosheets with 2D pyrochlore structure obtained from $Cs_{6+x}W_{11}O_{36}$, few studies on the photochromism of exfoliated nanosheets have been reported presumably because of the difficulty in synthesizing the nanosheets. The obtained nanosheets exhibited a reversible color change in response to UV irradiation, and their coloration efficiency was higher than that of hydrated WO_3 nanoparticles.[10] The superior performance of these materials motivates us to further explore chromogenic nanosheets with different chemical compositions and structures, which will lead to highly enhanced properties. In this study, we report the synthesis of 2D bronze tungstate nanosheets derived from $Rb_4W_{11}O_{35}$ and highlight their photochromic properties.

EXPERIMENTAL SECTION

Materials Synthesis. Layered rubidium tungstate, $Rb_4W_{11}O_{35}$, was synthesized as a starting material by heating a mixture of Rb_2CO_3 and WO_3 (2:11 by molar ratio) at 850 °C for 12 h in air. A total 1 g of the obtained $Rb_4W_{11}O_{35}$ was treated with 100 cm^3 of concentrated HCl for 120 h. The acid solution was replaced every day by decantation. The acid treatment produced a layered protonic rubidium tungstate with the chemical formula $H_{1.6}Rb_{2.4}W_{11}O_{35}{\cdot}nH_2O$ (n varies with humidity). A sample corresponding to 0.14 mmol of $H_{1.6}Rb_{2.4}W_{11}O_{35}$ was added to 100 cm^3 of a tetrabutylammonium hydroxide (TBAOH) solution and shaken vigorously for 10 days. The concentration of

Received: August 23, 2011
Published: December 22, 2011

   dx.doi.org/10.1021/ic201834y | *Inorg. Chem.* 2012, 51, 1540−1543

TBAOH in the solution was controlled such that the TBA^+-to-H^+ ratio, where H^+ is the ion-exchangeable proton content in the layered protonic tungstate, varied between $TBA^+/H^+ = 0.5$ and 10 to optimize the degree of exfoliation. Yellowish suspensions were produced at TBA^+/H^+ ratios of 1−2. The suspension obtained at $TBA^+/H^+ = 1$ (a 2.3 mmol dm^{-3} TBAOH solution was used) was considered the best condition and was used for further characterization after separation of a readily sedimented material of a nonexfoliated component via centrifugation at 2000 rpm for 30 min. A yield of the nanosheets in the suspension was roughly estimated on the basis of an ignition test; a volume of 5 cm^3 of the nanosheet suspension was completely dried and subsequently heated at 500 °C to remove water and organic components and convert them into anhydrous oxide. A weight of the ignited residue with respect to the initially added $H_{1.6}Rb_{2.4}W_{11}O_{35}$ (0.02 g) is taken as a yield of the nanosheets.

Film Fabrication. A silicon wafer was cleaned to obtain a hydrophilic surface by dipping it in a mixed solution of concentrated HCl and CH_3OH (1:1 by volume) and, subsequently, in a concentrated H_2SO_4 solution. The substrate was immersed in an aqueous solution of poly(diallyldimethylammonium chloride) (pH = 9; 2.5 g dm^{-3}) for 10 min to precoat the surface. Next, it was dipped into a colloidal suspension of negatively charged nanosheets (0.4 g dm^{-3}) for 10 min to assemble a monolayer film in which the tungstate nanosheets were adsorbed onto the substrate surface via electrostatic self-assembly.

A volume of 1 cm^3 of the tungstate nanosheet suspension (concentration: 2 g dm^{-3}) was added to a volume of 5 cm^3 of aqueous poly(vinyl alcohol) (PVA) solution (10%), providing a viscous mixture. Next, the mixture was cast directly onto a thin glass plate. After drying at room temperature for several days, a uniform film showing good transparency was obtained.

Measurements and Analysis. Powder X-ray diffraction (XRD) data were collected using a Bragg−Brentano-type diffractometer (Rigaku Rint 2000) with Cu Kα radiation (λ = 0.154 05 nm). Transmission electron microscopy (TEM) was performed with a JEOL 2010 microscope operated at an accelerating voltage of 200 kV. Specimens for the observations were prepared by directly placing droplets of the diluted nanosheet suspension onto a holey collodion-supported copper grid. Tapping-mode atomic force microscopy (AFM; Seiko Instruments SPA400) with a silicon-tip cantilever (20 N m^{-1}) was used to characterize the morphological features of the nanosheets deposited on a flat substrate. Optical absorption spectra for the diluted nanosheet suspensions in a quartz cell with 1-cm path length were recorded on a Hitachi U-4100 spectrophotometer.

The photochromism of the nanosheet suspension was assessed using a sealed quartz cell with a 1-cm path length. The suspension was diluted with ultrapure water to a concentration of 1.4×10^{-4} mol dm^{-3} (pH ~5.6). After the suspension was bubbled with N_2 gas, the cell was tightly sealed using a flexible paraffin film. A 200 W Hg−Xe lamp (San-ei Electric, UVF-S203) was used as an excitation source in the photochromism test of the nanosheet suspension and the nanosheet/PVA film. The light intensity at a bright line of 546 nm was 5.8 mW cm^{-2} nm^{-1}.

Chemical Analysis. A weighed amount of the powder samples of layered tungstate and its acid-exchanged product was melted in a mixture of Na_2CO_3 and H_3BO_3 by heating. The cooled material was dissolved with a 6 mol dm^{-3} HCl aqueous solution. The obtained solution was analyzed for rubidium by atomic absorption spectrometry (Hitachi Z-2300) and for tungsten by inductively coupled plasma atomic emission spectrometry (Seiko Instruments SPS-3500). Mass loss up to 500 °C as measured by thermogravimetry (Rigaku Thermo Plus TG 8120) was used to deduce the water content in the protonated derivatives.

RESULTS AND DISCUSSION

A starting sample of $Rb_4W_{11}O_{35}$ was synthesized by heating a mixture of Rb_2CO_3 and WO_3 (2:11 in molar ratio) at 850 °C in air. Its XRD data could be indexed based on an orthorhombic structure (see Figure 1a). The refined unit cell parameters, a = 1.4653(3) nm, b = 2.568(3) nm, and c = 0.7684(3) nm, are in good agreement with those reported for $Rb_4W_{11}O_{35}$.[12] Rb^+/H^+ exchange was attempted by treating the sample with a concentrated HCl solution for 120 h. A slight shift in the series of basal-plane diffraction peaks to lower angles was observed (Figure 1b). The refined parameters of the product were a = 1.464(1) nm, b = 2.578(2) nm, and c = 0.764(2) nm, suggesting that the crystal structure remained practically unchanged. Chemical analysis revealed the removal of ~40% of Rb^+, giving a chemical formula of $H_{1.6}Rb_{2.4}W_{11}O_{35}\cdot nH_2O$ (n varies with humidity). On the basis of the hypothetical structure of this compound, 75% of the Rb^+ is confined in a bronze-type tunnel composed of six-membered rings of WO_6 octahedra. The remaining Rb^+ ions (25%) are accommodated in the interlayer gallery and are believed to be preferentially exchanged with protons or oxonium ions upon acid exchange. The chemical analysis results suggest that some of the tunnel sites are available for the ion-exchange reaction as well.

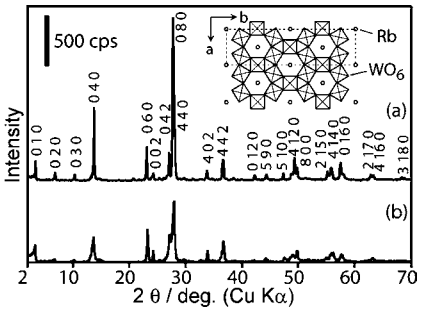

Figure 1. XRD patterns for (a) the starting material and (b) the protonated derivative. Inset: ideal structure of $Rb_4W_{11}O_{35}$ projected along the c axis.

The proton-exchanged layered tungstate was mixed into an aqueous TBAOH solution at ambient temperature to induce exfoliation. The dose of TBAOH was adjusted to be equivalent to the proton content in the solid. After shaking for 10 days, a yellowish suspension was formed. The yield of the colloidal tungstate was estimated to be 50% on an ignition test after separation of the unreacted residue by mild centrifugation at 2000 rpm for 30 min.

TEM was used to visualize the ultimate 2D morphology of a colloidal sample deposited on a copper grid. The typical image shown in Figure 2a depicts a sheet with sharp edges and a lateral dimension in the submicrometer range. Such a faint but uniform contrast usually stems from a molecularly thin

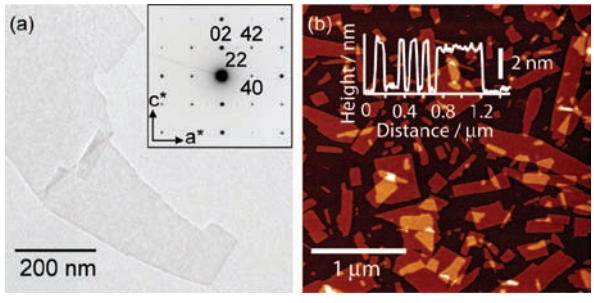

Figure 2. (a) TEM micrograph of the colloidal nanosheet dropped on a copper grid and its selected-area electron diffraction pattern and (b) AFM image of the tungstate nanosheets on a silicon substrate. Inset in right panel: height profile along its abscissa axis.

dx.doi.org/10.1021/ic201834y | Inorg. Chem. 2012, 51, 1540−1543

structure that allows the facile passage of the electron beam. Note that portions with a denser contrast can be ascribed to folding of the sheet. Electron diffraction revealed a single-crystal pattern possessing symmetrical and sharp spots. The pattern can be assigned to a rectangular unit cell of 1.4 nm × 0.78 nm compatible with the 2D symmetry of the parent material.

AFM images of the tungstate nanosheets adsorbed on a silicon substrate coated with cationic polymers, such as that shown in Figure 2b, showed numerous sheets with a thickness of approximately 3 nm and a sheet size on the micrometer scale. The observed height is consistent with the thickness of the host layer estimated from the ideal structure of $Rb_4W_{11}O_{35}$;[12] the crystallographic thickness of the host layer, including the ionic size of the two outermost oxygen atoms (~0.28 nm), gives a value of approximately 2.5 nm. As is often the case with other oxide nanosheets, the small difference between the experimental data and the crystallographic thickness may be explained in terms of charge-compensating cationic species and/or water molecules adsorbed on the nanosheet surface.[13] These results suggest that unilamellar nanosheet crystallites of tungstate with a 2D bronze structure were successfully obtained as a monodispersed colloidal species.

Figure 3 depicts the UV−vis diffuse-reflectance spectrum for the protonated derivative and the absorption spectrum for the

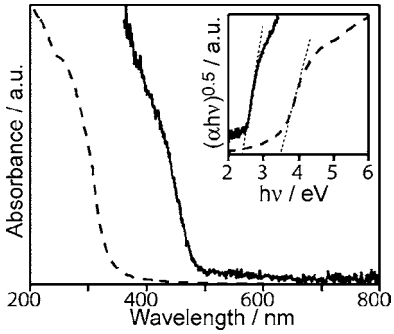

Figure 3. UV−vis diffuse-reflectance spectrum of the proton-exchanged tungstate (solid line) and absorption spectrum of the nanosheet suspension (broken line). Inset : plot of $(\alpha h\nu)^{0.5}$ against $h\nu$.

colloidal suspension of the tungstate nanosheets. The exfoliated nanosheets show an intense UV absorption band at a wavelength of 380 nm and below. A plot of the absorbance at 250 nm as a function of the nanosheet concentration shown in Figure 4 revealed a linear relationship between them. This supports that the parent layered protonic tungstate was delaminated into monodispersed colloids, i.e., exfoliated nanosheets. The molar extinction coefficient obtained from a gradient of the approximate line is 7×10^4 mol^{-1} dm^3 cm^{-1} at 250 nm. The square root of the absorption coefficient α times the photon energy $h\nu$ is plotted against the photon energy (see Figure 3, inset). The upsurge portion of $(\alpha h\nu)^{0.5}$ is fitted by the straight dotted line, indicating that the tungstate system has an indirect electronic transition near the band gap. The optical band-gap energies for the precursor and the tungstate nanosheets can be derived as approximately 2.4 and 3.5 eV, respectively, from the intersection of the dotted line and the abscissa axis. The distinctive blue shift may be explained by the quantum size effect arising from the nanoscale dimension of the material, which can be observed in quantized tungstate materials with dimensions of less than 5 nm.[4c,d,10] Therefore,

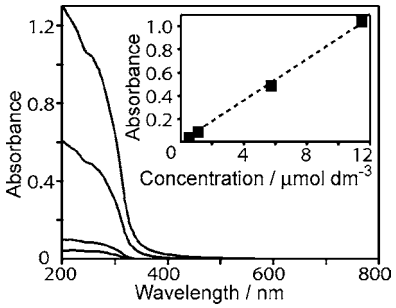

Figure 4. UV−vis absorption spectra obtained from the colloidal suspension of the tungstate nanosheets at various concentrations. Inset: plot of the absorbance at 250 nm against the concentration of the suspension (R^2 = 0.998).

the 2D bronze tungstate nanosheets can be described as a new family of wide-gap tungstate semiconductors.

It is of interest to examine the photochromic properties of the 2D bronze tungstate nanosheets, which feature a linkage of WO_6 octahedra similar to that of tungsten bronze (A_xWO_3; A is proton or alkali-metal ions) that is known as a good candidate for an inorganic chromogen. Figure 5 shows the UV−vis

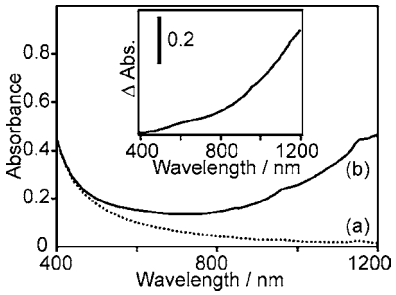

Figure 5. UV−vis absorption spectra obtained from the nanosheet suspension (a) before and (b) after UV irradiation. Inset: difference in absorbance between virgin and colored states.

absorption spectra for the nanosheet suspension before and after UV irradiation. Because of the emergence of an absorption upsurge above 400 nm, the turbid suspension showing the weak light scattering turned bluish black after 10 min of UV illumination, and the coloration was visually saturated after 40 min under this condition. The absorbance gain estimated from the difference in the absorbance between the pristine and colored states, ΔAbs, provides a clearer vision of the color change, indicating that the 2D bronze nanosheet functions as a photochromogen similar to the 2D pyrochlore nanosheet reported previously.[10] In this study, we compare the coloration efficiency between the 2D bronze and 2D pyrochlore nanosheets on the basis of ΔAbs normalized in terms of the cell length and concentration, neglecting the slight difference in their spectral shape. ΔAbs for the former suspension possessing a concentration of 1.4×10^{-4} mol dm^{-3} in a 1-cm cell reached ~0.4 at 1100 nm. The latter system yielded a ΔAbs of ~0.09 at a concentration of 6.7×10^{-5} mol dm^{-3} in a 1-cm cell unit.[10] On the basis of this comparison, the coloration rate of the 2D bronze nanosheet is at least two times better at the measured wavelength. This may be associated with possibly higher efficiency of the intervalence charge-transfer transition and/or accessibility of the ion-exchangeable tunnel structure of the 2D bronze nanosheet as a surface site. This finding means that the present nanosheet has the top-ranked photochromogenic

dx.doi.org/10.1021/ic201834y | Inorg. Chem. 2012, 51, 1540−1543

performance among a variety of tungstate materials in the near-IR spectrum.

To estimate the photochromic response over a wider range covering near-IR, a film sample of the 2D bronze nanosheets was fabricated using PVA, which acts as a proton-donor additive in the coloration of the WO_3 system.[5] The addition of the PVA solution to the nanosheet suspension enhanced the viscosity without any visible change regarding the dispersion state of the nanosheet. Unlike the case with a nanosheet-restacked film readily obtained by drying a droplet of the nanosheet suspension on a glass substrate, a droplet of the nanosheet/PVA suspension on a glass substrate yielded a uniform and transparent film, in which the nanosheets were well-dispersed. As for the nanosheet-restacked film, a series of basal diffraction peaks originating from a stacked structure with an interlayer distance of d = 3.8 nm was observed (see Figure 6). The obtained d value is significantly larger than the basal spacing (b axis) of $Rb_4W_{11}O_{35}$. This expansion can be explained by accommodation of hydrated TBA^+ (the molecular size of TBA^+ is ~0.9 nm) between 2D bronze-type tungstate layers. On the other hand, the nanosheet/PVA film showed a broad halo pattern without apparent basal peaks. Besides it, two broad XRD peaks centered at 19.6° and 27.9° assignable to PVA in crystalline and hydrogel forms,[14] respectively, were detected. This result suggests that the tungstate nanosheets were randomly dispersed in the PVA matrix. Figure 7 shows that the nanosheet/PVA film exhibited the same coloration behavior as the suspension system. Interestingly, the coloration degree is saturated at ~1800 nm without a distinctive absorption peak at 600−1000 nm as a common feature for most amorphous tungstates.[4,5] This spectral profile may be unique to crystalline tungstate chromogens because similar absorption can be observed in the reversible coloration of microcrystalline tungstate.[15,16] Thus, the photochromic properties of the 2D bronze tungstate nanosheets obtained in this study are characterized by intense UV absorption and optically switchable IR absorption, which may be useful for practical applications, such as cutoff filters and heat-absorbing films.

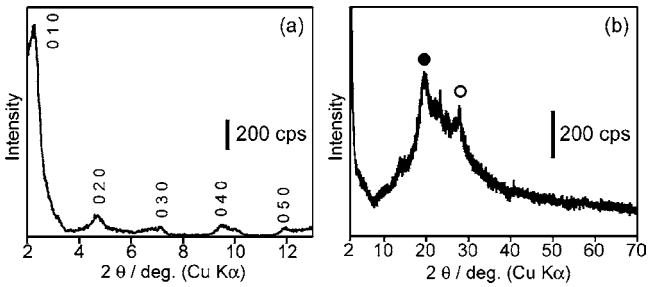

Figure 6. XRD patterns for (a) a nanosheet-restacked film and (b) a nanosheet/PVA composite film. (● and ○) XRD peaks of PVA in crystalline and hydrogel forms, respectively.

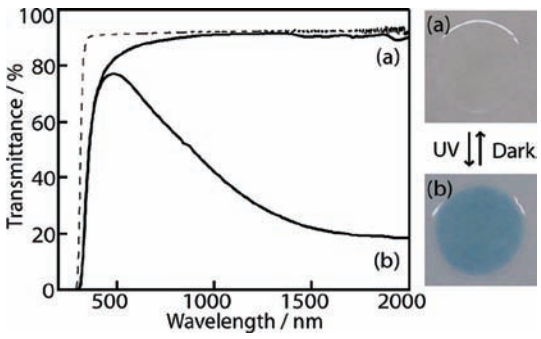

Figure 7. Optical absorption spectra of the nanosheet/PVA film for (a) pristine and (b) colored states. The dotted profile is for a glass substrate.

CONCLUSION

We have succeeded in synthesizing a new class of highly crystalline tungstate nanosheets via the soft-chemical delamination of $Rb_4W_{11}O_{35}$. The obtained nanosheets exhibited photoinduced coloration peculiar to crystalline systems and are promising as a unique class of inorganic chromogens that can be used not only for photochromic windows but also for electrochromic devices.

AUTHOR INFORMATION

Corresponding Author

*E-mail: Sasaki.Takayoshi@nims.go.jp (T.S.), K_F@aug.rikadai.jp (K.F.). Fax: +81-29-854-9061.

ACKNOWLEDGMENTS

This work was supported, in part, by WPI Initiative on Materials Nanoarchitectonics, MEXT, Japan, CREST of JST, and Grant-in-Aid for Young Scientists (B) of JSPS.

REFERENCES

(1) Nenadovic, M. T.; Rajh, T.; Micici, O. I.; Nozik, A. J. *J. Phys. Chem.* **1984**, *88*, 5827.
(2) Subbarao, E. C. *Ferroelectrics* **1973**, *5*, 267.
(3) Stanley, R. K.; Morris, R. C.; Moulton, W. G. *Phys. Rev. B* **1979**, *20*, 1903.
(4) (a) Deb, S. K. *Philos. Mag.* **1973**, *27*, 801. (b) Shigesato, Y. *Jpn. J. Appl. Phys.* **1991**, *30*, 1457. (c) Bedja, I.; Hotchandai, S.; Kamat, P. V. *J. Phys. Chem.* **1993**, *97*, 11064. (d) He, Y.; Wu, Z.; Fu, L.; Li, C.; Miao, Y.; Cao, L.; Fan, H.; Zou, B. *Chem. Mater.* **2003**, *15*, 4039.
(5) (a) Kuboyama, K.; Hara, K.; Matushige, K. *Jpn. J. Appl. Phys.* **1994**, *33*, 4135. (b) Yano, S.; Kurita, K.; Iwata, K.; Furukawa, T.; Kodomari, M. *Polymer* **2003**, *44*, 3515.
(6) Bange, K.; Gambke, T. *Adv. Mater.* **1990**, *2*, 10.
(7) Tatsuma, T.; Saitoh, S.; Ngaotrakanwiwat, P.; Ohko, Y.; Fujishima, A. *Langmuir* **2002**, *18*, 7777.
(8) Walker, G. F. *Nature* **1960**, *187*, 312.
(9) (a) Treacy, M. M.; Rice, S. B.; Jacobson, A. J.; Lewandowski, J. T. *Chem. Mater.* **1990**, *2*, 279. (b) Sasaki, T.; Watanabe, M.; Hashizume, H.; Yamada, H.; Nakazawa, H. *J. Am. Chem. Soc.* **1996**, *118*, 8329. (c) Schaak, R. E.; Mallouk, T. E. *Chem. Commun.* **2002**, 706. (d) Ma, R.; Sasaki, T. *Adv. Mater.* **2010**, *22*, 5082.
(10) Fukuda, K.; Akatsuka, K.; Ebina, Y.; Ma, R.; Takada, K.; Nakai, I.; Sasaki, T. *ACS Nano* **2008**, *2*, 1689.
(11) Novoselov, K. S.; Geim, A. K.; Morozov, S. V.; Jiang, D.; Zhang, Y.; Dubonos, S. V.; Grigorieva, I. V.; Firsov, A. A. *Science* **2004**, *306*, 666.
(12) Solodovnikov, S. F.; Ivannikova, N. V.; Solodovnikova, Z. A.; Zolotova, E. S. *Inorg. Mater.* **1998**, *34*, 845.
(13) Sasaki, T.; Ebina, Y.; Kitami, Y.; Watanabe, M.; Oikawa, T. *J. Phys. Chem. B* **2001**, *105*, 6116.
(14) Ricciardi, R.; Auriemma, F.; Rosa, C. D.; Lauprêtre, F. *Macromolecules* **2004**, *37*, 1921.
(15) Deneuville, A.; Gérard, P. *J. Electron. Mater.* **1978**, *7*, 559.
(16) Svensson, J. S. E. M.; Granqvist, C. G. *Appl. Phys. Lett.* **1984**, *45*, 828.